

Exclusive production of lepton, quark and meson pairs in peripheral ultrarelativistic heavy ion collisions

A. Szczurek ^{a b}

^aUniversity of Rzeszów, PL-35-959 Rzeszów, Poland

^bInstitute of Nuclear Physics, PL-31-342 Cracow, Poland

We discuss exclusive production of lepton-antilepton, quark-antiquark, $\pi\pi$ and $\rho^0\rho^0$ pairs in ultraperipheral, ultrarelativistic heavy-ion collisions.

The cross sections for exclusive production of pairs of particles is calculated in Equivalent Photon Approximation (EPA). Realistic (Fourier transform of charge density) charge form factors of nuclei are used and the corresponding results are compared with the cross sections calculated with monopole form factor used in the literature. Absorption effects are discussed and quantified. The cross sections obtained with realistic form factors are significantly smaller than those obtained with the monopole form factors.

The cross section for exclusive $\mu^+\mu^-$ production in nucleus - nucleus collisions are calculated and some differential distributions are shown. The effect of absorption is bigger for large muon rapidities and/or large muon transverse momenta. We present predictions for LHC.

We calculate cross section for exclusive production of $\pi^+\pi^-$ and $\pi^0\pi^0$ pairs. The elementary process $\gamma\gamma \rightarrow \pi\pi$ is discussed in detail. We concentrate on high- p_t processes. We consider pQCD Brodsky-Lepage processes or alternatively hand-bag mechanism. The nuclear cross section is calculated within b-space EPA for RHIC and LHC.

Similar analysis is performed for $\rho^0\rho^0$ production, where the elementary cross section is less known. Our analysis includes a close-to-threshold enhancement of the cross section. The cross section for the low-energy phenomenon is parametrized and the high-energy cross section is calculated in a simple Regge model. Predictions for heavy ion collisions are presented.

The cross section for exclusive heavy quark and heavy antiquark pair ($Q\bar{Q}$) production in heavy ion collisions is calculated for the LHC energy $\sqrt{s_{NN}} = 5.5$ TeV. Here we consider only processes with photon-photon interactions and omit diffractive contributions. We include both $Q\bar{Q}$, $Q\bar{Q}g$ and $Q\bar{Q}q\bar{q}$ final states as well as photon single-resolved components. The different components give contributions of the same order of magnitude to the nuclear cross section. The cross sections found here are smaller than those for the diffractive photon-pomeron mechanism and larger than diffractive pomeron-pomeron discussed in the literature.

1. Introduction

It was shown in several review articles [1] that the ultrarelativistic collisions of heavy ions provide a nice opportunity to study photon-photon collisions. This is due to the enhancement caused by the large charge of the colliding ions. Parametrically the cross section is proportional to $Z_1^2 Z_2^2$ which is a huge number. It was discussed recently that the inclusion of realistic charge distributions in nuclei lowers the cross section compared to the naive predictions. Recently we have studied the

production of $\rho^0\rho^0$ pairs [2], of $\mu^+\mu^-$ pairs [3], of heavy-quark heavy-antiquark pairs [4] as well as of $D\bar{D}$ meson pairs [5].

Here we shall briefly summarize the recent works.

2. Formalism

2.1. Equivalent Photon Approximation

The equivalent photon approximation is a standard semi-classical alternative to the Feynman rules for calculating cross sections of electromag-

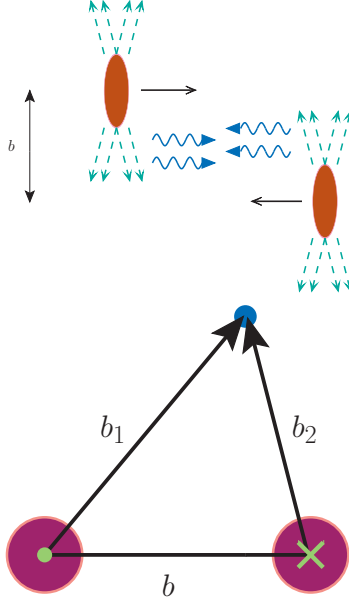


Figure 1. A schematic picture of the collision and the quantities used in the impact parameter calculation.

netic interactions [9]. This picture is illustrated in Fig. 1 where one can see a fast moving nucleus with the charge Ze . Due to the coherent action of all protons in the nucleus, the electromagnetic field surrounding (the dashed lines are lines of electric force for a particles in motion) the ions is very strong. This field can be viewed as a cloud of virtual photons. In the collision of two ions, these quasireal photons can collide with each other and with the other nucleus. The strong electromagnetic field is a source of photons that can induce electromagnetic reactions on the second ion. We consider very peripheral collisions i.e. we assume that the distance between nuclei is bigger than the sum of radii of the two nuclei. Fig. 1 explains also the quantities used in the impact parameter calculation. We can see a view in the plane perpendicular to the direction of motion of the two ions. In order to calculate the cross section of a process it is convenient to introduce the following kinematic variables:

- $x = \omega/E_A$, where ω energy of the photon

and the energy of the nucleus

- $E_A = \gamma Am_{proton} = \gamma M_A$ where M_A is the mass of the nucleus and E_A is the energy of the nucleus

The total cross section can be calculated by the convolution:

$$\sigma(AA \rightarrow c_1 c_2 AA; s_{AA}) = \int \hat{\sigma}(\gamma\gamma \rightarrow c_1 c_2; W_{\gamma\gamma} = \sqrt{x_1 x_2 s_{AA}}) dn_{\gamma\gamma}(x_1, x_2, \mathbf{b}). \quad (1)$$

The luminosity function can be expressed in term of flux factors of photons prescribed to each of the nucleus.

$$dn_{\gamma\gamma}(\omega_1, \omega_2, \mathbf{b}) = \int S_{abs}^2(\mathbf{b}) d^2 \mathbf{b}_1 N(\omega_1, \mathbf{b}_1) d^2 \mathbf{b}_2 N(\omega_2, \mathbf{b}_2) \frac{d\omega_1}{\omega_1} \frac{d\omega_2}{\omega_2}. \quad (2)$$

The presence of the absorption factor $S_{abs}^2(\mathbf{b})$ assures that we consider only peripheral collisions, when the nuclei do not undergo nuclear breakup. In the first approximation this can be taken into account as:

$$S_{abs}^2(\mathbf{b}) = \theta(\mathbf{b} - 2R_A) = \theta(|\mathbf{b}_1 - \mathbf{b}_2| - 2R_A). \quad (3)$$

Thus in the present case, we concentrate on processes with final nuclei in the ground state. The electric field force can be expressed through the charge form factor of the nucleus [3].

The total cross section for the $AA \rightarrow c_1 c_2 AA$ process can be factorized into an equivalent photons spectra and the $\gamma\gamma \rightarrow c_1 c_2$ subprocess cross section as

$$\sigma(AA \rightarrow c_1 c_2 AA; s_{AA}) = \int \hat{\sigma}(\gamma\gamma \rightarrow c_1 c_2; \sqrt{4\omega_1 \omega_2}) \theta(|\mathbf{b}_1 - \mathbf{b}_2| - 2R_A) N(\omega_1, \mathbf{b}_1) N(\omega_2, \mathbf{b}_2) d^2 \mathbf{b}_1 d^2 \mathbf{b}_2 \frac{d\omega_1}{\omega_1} \frac{d\omega_2}{\omega_2}. \quad (4)$$

We introduce the invariant mass of the $\gamma\gamma$ system: $W_{\gamma\gamma} = \sqrt{4\omega_1 \omega_2}$. Additionally, we define $Y = \frac{1}{2}(y_{c_1} + y_{c_2})$ rapidity of the outgoing $c_1 c_2$ system which is produced in the photon-photon collision. Making the following transformations:

$$\omega_1 = \frac{W_{\gamma\gamma}}{2} e^Y, \quad \omega_2 = \frac{W_{\gamma\gamma}}{2} e^{-Y}, \quad (5)$$

$$\frac{d\omega_1}{\omega_1} \frac{d\omega_2}{\omega_2} = \frac{2}{W_{\gamma\gamma}} dW_{\gamma\gamma} dY, \quad (6)$$

$$d\omega_1 d\omega_2 \rightarrow dW_{\gamma\gamma} dY \left| \frac{\partial(\omega_1, \omega_2)}{\partial(W_{\gamma\gamma}, Y)} \right| = \frac{W_{\gamma\gamma}}{2}, \quad (7)$$

formula (4) can be written in an equivalent way as

$$\begin{aligned} \sigma(AA \rightarrow c_1 c_2 AA; s_{AA}) = & \int \hat{\sigma}(\gamma\gamma \rightarrow c_1 c_2; W_{\gamma\gamma}) \theta(|\mathbf{b}_1 - \mathbf{b}_2| - 2R_A) \\ & N(\omega_1, \mathbf{b}_1) N(\omega_2, \mathbf{b}_2) \\ & \times d^2\mathbf{b}_1 d^2\mathbf{b}_2 \frac{2}{W_{\gamma\gamma}} dW_{\gamma\gamma} dY. \end{aligned} \quad (8)$$

Finally the cross section can be expressed as the five-fold integral:

$$\begin{aligned} \sigma(AA \rightarrow c_1 c_2 AA; s_{AA}) = & \int \hat{\sigma}(\gamma\gamma \rightarrow \mu^+ \mu^-; W_{\gamma\gamma}) \theta(|\mathbf{b}_1 - \mathbf{b}_2| - 2R_A) \\ & \times N(\omega_1, \mathbf{b}_1) N(\omega_2, \mathbf{b}_2) \\ & 2\pi b_m db_m db_x db_y \frac{W_{\gamma\gamma}}{2} dW_{\gamma\gamma} dY, \end{aligned} \quad (9)$$

where $\vec{b}_x \equiv (b_{1x} + b_{2x})/2$, $\vec{b}_y \equiv (b_{1y} + b_{2y})/2$ and $\vec{b}_m = \vec{b}_1 - \vec{b}_2$ have been introduced. The formula above is used to calculate the total cross section for the $AA \rightarrow AA c_1 c_2$ reaction as well as distributions in $b = b_m$, $W_{\gamma\gamma} = M_{c_1 c_2}$ and $Y(c_1 c_2)$.

Different forms of form factors are used in the literature. We compare the equivalent photon spectra for realistic charge distribution and for the case of monopole form factor.

2.2. Charge form factor of nuclei

The charge distribution in nuclei is usually obtained from elastic scattering of electrons from nuclei [7]. The charge distribution obtained from those experiments is often parametrized with the help of two-parameter Fermi model [8]:

$$\rho(r) = \rho_0 \left(1 + \exp\left(\frac{r-c}{a}\right) \right)^{-1}, \quad (10)$$

where c is the radius of the nucleus, a is the so-called diffuseness parameter of the charge density.

Fig. 2 shows the charge density normalized to unity. The correct normalization is: $\rho_{0,Au}(0) =$

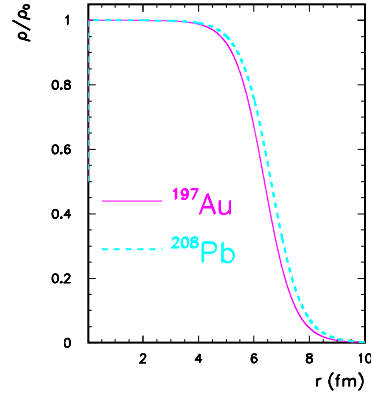


Figure 2. The ratio of ρ the charge distribution to ρ_0 the density in the center of nucleus.

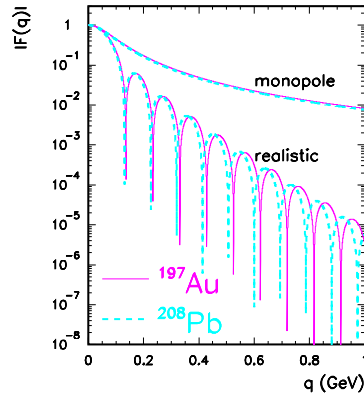


Figure 3. The moduli of the charge form factor $F_{em}(q)$ of the ^{197}Au and ^{208}Pb nuclei for realistic charge distributions. For comparison we show the monopole form factor for the same nuclei.

$\frac{0.1694}{A} fm^{-3}$ for Au and $\rho_{0,Pb}(0) = \frac{0.1604}{A} fm^{-3}$ for Pb.

The form factor is the Fourier transform of the charge distribution [7]:

$$F(q) = \int \frac{4\pi}{q} \rho(r) \sin(qr) r dr. \quad (11)$$

Fig. 3 shows the moduli of the form factor as a function of momentum transfer. Here one can see many oscillations characteristic for relatively sharp edge of the nucleus. The results are depicted for the gold (solid line) and lead (dashed line) nuclei for realistic charge distribution. For comparison we show the monopole form factor used in the literature. The two form factors coincide only in a very limited range of q .

The monopole form factor [11]:

$$F(q^2) = \frac{\Lambda^2}{\Lambda^2 + q^2}. \quad (12)$$

leads to simplification of many formulae for production of pairs of particles via photon-photon subprocess in nucleus-nucleus collisions. In our calculation Λ is adjusted to reproduce root mean square radius $\Lambda = \sqrt{\frac{6}{\langle r^2 \rangle}}$ with the help of experimental data [8].

3. Examples

In the following we shall discuss several examples considered by us recently. We shall discuss individual processes in respective subsections.

3.1. Exclusive production of $\mu^+\mu^-$ pairs

For dimuon production the elementary cross section can be calculated within QED.

In Ref.[3] we have presented several distributions in muon rapidity and transverse momentum for RHIC and LHC experiments, including experimental acceptances. Here we wish to present only one example.

The ALICE collaboration can measure only forward muons with pseudorapidity $4 < \eta < 5$ and has relatively low cut on muon transverse momentum $p_t > 2$ GeV. In Fig.4 (left panel) we show invariant mass distribution of dimuons for monopole and realistic form factors including the cuts of the ALICE apparatus. The bigger invariant mass the bigger the difference between the two results. The same is true for distributions in muon transverse momenta (see the right panel).

3.2. Exclusive production of $\pi^+\pi^-$ pairs

Basic diagrams of the Brodsky and Lepage formalism are shown in Fig. 5. The invariant ampli-

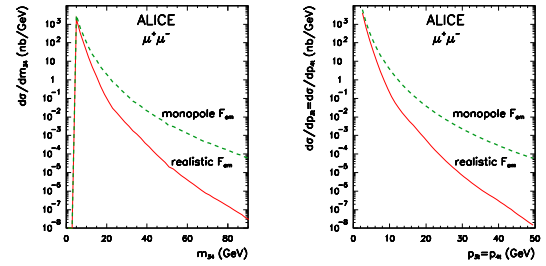


Figure 4. $\frac{d\sigma}{dW_{\gamma\gamma}}$ (left) and $\frac{d\sigma}{dp_{3t}} = \frac{d\sigma}{dp_{4t}}$ (right) for ALICE conditions: $y_3, y_4 = (3, 4)$, $p_{3t}, p_{4t} \geq 2$ GeV.

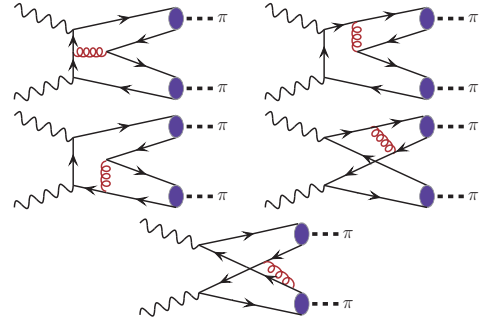


Figure 5. Feynman diagrams describing the $\gamma\gamma \rightarrow (q\bar{q})(q\bar{q}) \rightarrow \pi\pi$ amplitude in the LO pQCD.

tude for the initial helicities of two photons can be written as the following convolution:

$$\mathcal{M}(\lambda_1, \lambda_2) = \int_0^1 dx \int_0^1 dy \phi_\pi(x, \mu_x^2) T_H^{\lambda_1 \lambda_2}(x, y, \mu^2) \phi_\pi(y, \mu_y^2), \quad (13)$$

where $\mu_x = \min(x, 1-x) \sqrt{s(1-z^2)}$, $\mu_y = \min(y, 1-y) \sqrt{s(1-z^2)}$; $z = \cos \theta$ [12]. We take the helicity dependent hard scattering amplitudes from Ref. [13]. These scattering amplitudes are different for $\pi^+\pi^-$ and $\pi^0\pi^0$. The distribution amplitudes are subjected to the ERBL pQCD evolution [15,16]. The scale dependent quark distribution amplitude of the pion can be expanded

in term of the Gegenbauer polynomials:

$$\phi_\pi(x, \mu^2) = \frac{f_\pi}{2\sqrt{3}} 6x(1-x) \sum_{n=0}^{\infty'} C_n^{3/2}(2x-1) a_n(\mu^2). \quad (14)$$

f_π above is the pion decay constant.

Different distribution amplitudes have been used in the past. Wu and Huang [18] proposed recently a new distribution amplitude (based on a certain light-cone wave function):

$$\begin{aligned} \phi_\pi(x, \mu_0^2) &= \frac{\sqrt{3}A m_q \beta}{2\sqrt{2}\pi^{3/2} f_\pi} \sqrt{x(1-x)} \\ &\left(1 + B \times C_2^{3/2}(2x-1)\right) \\ &\left(\text{Erf}\left[\sqrt{\frac{m_q^2 + \mu_0^2}{8\beta^2 x(1-x)}}\right] - \text{Erf}\left[\sqrt{\frac{m_q^2}{8\beta^2 x(1-x)}}\right]\right). \end{aligned} \quad (15)$$

This pion distribution amplitude at the initial scale is controlled by the parameter B. They have found that the BABAR data for pion transition form factor at low and high transferred four-momentum squared regions can be described by setting B to be around 0.6. This pion distribution amplitude is rather close to the well know Chernyak-Zhitnitsky [17] distribution amplitude ($\phi_{\pi CZ} = 30x(1-x)(2x-1)^2$). In the following we shall use $B = 0.6$ and $m_q = 0.3$ GeV. Then $A = 16.62$ GeV⁻¹ and $\beta = 0.745$ GeV.

The total (angle integrated) cross section for the process can be expressed in terms of the amplitude of the process discussed above as:

$$\sigma_{\gamma\gamma \rightarrow \pi\pi} = \int \frac{2\pi}{4 \cdot 64\pi^2 W^2} \frac{p}{q} \sum_{\lambda_1, \lambda_2} |\mathcal{M}(\lambda_1, \lambda_2)|^2 dz, \quad (16)$$

where the factor 4 is due to averaging over initial photon helicities.

The hand-bag model was proposed as an alternative for the leading term BL pQCD approach [19]. It is based on the philosophy that the present energies are not sufficient for the dominance of the leading pQCD terms. As in the case of BL pQCD the hand-bag approach applies at large Mandelstam variables $s \sim -t \sim -u$ i.e. at large momentum transfers. Diehl, Kroll and Vogt presented a sketchy derivation [19] obtaining that the angular dependence of the amplitude is $\propto 1/\sin^2 \theta$.

In this approach the ratio of the cross section for the $\pi^0\pi^0$ process to the $\pi^+\pi^-$ process does not depend on θ and is $\frac{1}{2}$. The nonperturbative object $R_{\pi\pi}(s)$ in the hand-bag amplitude, describing transition from a quark pair to a meson pair, cannot be calculated from first principles. In Ref. [19] the form factor was parametrized in terms of the valence and non-valence form factors as:

$$R_{\pi\pi}(s) = \frac{5}{9s} a_u \left(\frac{s_0}{s}\right)^{n_u} + \frac{1}{9s} a_s \left(\frac{s_0}{s}\right)^{n_s}. \quad (17)$$

The a_u , n_u , a_s and n_s values found from the fit in Ref. [19] slightly depend on energy. For simplicity we have averaged these values and used in the present calculations: $a_u = 1.375$ GeV², $n_u = 0.4175$, $a_s = 0.5025$ GeV² and $n_s = 1.195$.

In Ref.[6] we have discussed in detail elementary cross sections as a function of photon-photon energy and as a function of $\cos(\theta)$. Here we have room for presenting only nuclear cross sections calculated within EPA discussed in the theoretical section.

In Fig. 6 we show distribution in the two-pion invariant mass which by the energy conservation is also the photon-photon subsystem energy. For this figure we have taken experimental limitations usually used for the $\pi\pi$ production in e^+e^- collisions. In the same figure we show our results for the $\gamma\gamma$ collisions extracted from the e^+e^- collisions together with the corresponding nuclear cross sections for $\pi^+\pi^-$ (left panel) and $\pi^0\pi^0$ (right panel) production. We show the results for the standard BL pQCD approach and for the hand-bag approach.

By comparison of the elementary and nuclear cross sections we see a large enhancement of the order of 10^4 which is somewhat less than $Z_1^2 Z_2^2$ one could expect from a naive counting.

3.3. Exclusive production of $\rho^0\rho^0$ pairs

At low energies one observes a huge enhancement of the cross section for the elementary process $\gamma\gamma \rightarrow \rho^0\rho^0$ (see left panel of Fig.7). In the right panel we show predictions of a simple Regge-VDM model with parameters adjusted to the world hadronic data. More details about our model can be found in our original paper [2].

In Fig.8 we show distribution in $\rho^0\rho^0$ invariant mass (left panel) and the ratio of the cross section for realistic and monopole form factors.

3.4. Exclusive production of $c\bar{c}$

In Fig.9,10,11,12 we show photon-photon processes leading to the $Q\bar{Q}$ in the final state. In the following we shall discuss them one by one.

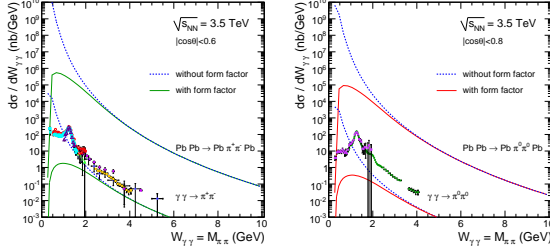


Figure 6. The nuclear (upper lines) and elementary (lower lines) cross section as a function of photon-photon subsystem energy $W_{\gamma\gamma}$ in the b-space EPA within the BL pQCD approach for the elementary cross section with Wu-Huang distribution amplitude. The angular ranges in the figure caption correspond to experimental cuts.

Let us start with the Born direct contribution. The leading-order elementary cross section for $\gamma\gamma \rightarrow Q\bar{Q}$ as a function of $W_{\gamma\gamma}$ takes a simple form which differs from that for $\gamma\gamma \rightarrow l^+l^-$ by color factors and fractional charges of quarks.

In the current calculation we take the following heavy quark masses: $m_c = 1.5$ GeV, $m_b = 4.75$ GeV. This formula can be directly used in the impact-parameter-space EPA. It is obvious that the final $Q\bar{Q}$ state cannot be observed experimentally due to the quark confinement and rather heavy mesons have to be observed instead. Presence of additional few light mesons is rather natural. This forces one to include more complicated final states.

In contrast to QED production of lepton pairs in photon-photon collisions, in the case of $Q\bar{Q}$ production one needs to include also higher-order QCD processes which are known to be rather significant. Here we include leading-order corrections only for the direct contribution. In α_s -order there are one-gluon bremsstrahlung diagrams ($\gamma\gamma \rightarrow Q\bar{Q}g$) and interferences of the Born diagram with self-energy diagrams (in $\gamma\gamma \rightarrow Q\bar{Q}$) and vertex-correction diagrams (in $\gamma\gamma \rightarrow Q\bar{Q}$). The relevant diagrams are shown in Fig.10. In the present analysis we follow the approach presented in Ref. [20]. The QCD corrections can be written as

$$\sigma_{\gamma\gamma \rightarrow Q\bar{Q}(g)}^{QCD}(W_{\gamma\gamma}) = N_c e_Q^4 \frac{2\pi\alpha_{em}^2}{W_{\gamma\gamma}^2} C_F \frac{\alpha_s}{\pi} f^{(1)}. \quad (18)$$

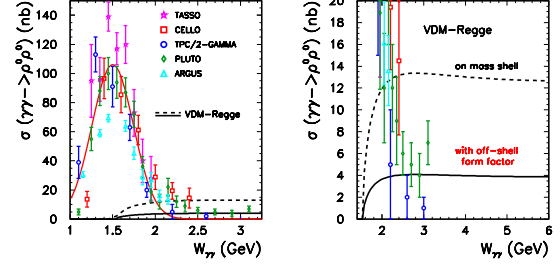


Figure 7. Elementary cross section for $\gamma\gamma \rightarrow \rho^0\rho^0$ reaction. The fit to the experimental data is shown in the left panel and our predictions for the high energy in the right panel.

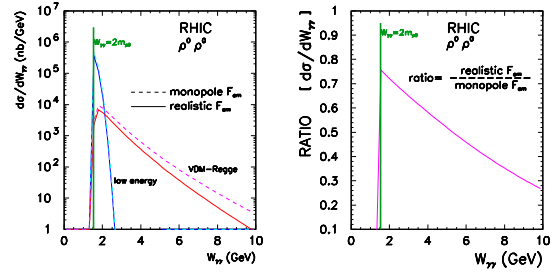


Figure 8. Distribution in the $\rho^0\rho^0$ invariant mass

The function $f^{(1)}$ is calculated using a code provided by the authors of Ref. [20]. In the present analysis the scale of α_s is fixed at $\mu^2 = 4m_Q^2$.

We include also the subprocess $\gamma\gamma \rightarrow Q\bar{Q}q\bar{q}$, where q (\bar{q}) are u , d , s , quarks (antiquarks). The cross section for this mechanism can be easily calculated in the color dipole framework [21,22]. In the dipole-dipole approach [22] the total cross section for the $\gamma\gamma \rightarrow Q\bar{Q}$ production can be expressed as

$$\begin{aligned} \sigma_{\gamma\gamma \rightarrow Q\bar{Q}}^{4q}(W_{\gamma\gamma}) &= \sum_{f_2 \neq Q} \int \left| \Phi^{Q\bar{Q}}(\rho_1, z_1) \right|^2 \left| \Phi^{f_2\bar{f}_2}(\rho_2, z_2) \right|^2 \\ &\quad \sigma_{dd}(\rho_1, \rho_2, x_{Qf}) d^2\rho_1 dz_1 d^2\rho_2 dz_2 \end{aligned}$$

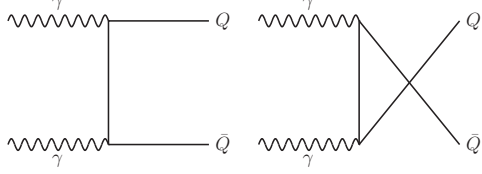


Figure 9. Representative diagrams for the Born amplitudes.

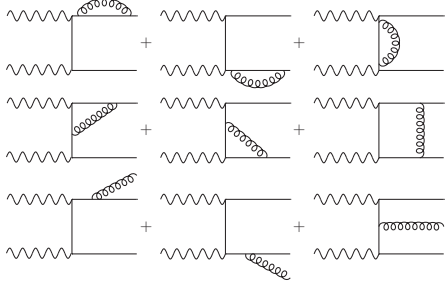


Figure 10. Representative diagrams for the leading-order QCD corrections.

$$+ \sum_{f_1 \neq Q} \int \left| \Phi^{f_1 \bar{f}_1}(\rho_1, z_1) \right|^2 \left| \Phi^{Q\bar{Q}}(\rho_2, z_2) \right|^2 \sigma_{dd}(\rho_1, \rho_2, x_{fQ}) d^2 \rho_1 dz_1 d^2 \rho_2 dz_2, \quad (19)$$

where $\Phi^{Q\bar{Q}}(\rho, z)$ are the quark – antiquark wave functions of the photon in the mixed representation and σ_{dd} is the dipole–dipole cross section. Eq.(19) is correct at sufficiently high energy $W_{\gamma\gamma} \gg 2m_Q$. At lower energies, the proximity of the kinematical threshold is a concern. In Ref. [21] a phenomenological saturation–model inspired parametrization for the azimuthal angle averaged dipole–dipole cross section has been proposed:

$$\sigma_{dd}^{a,b} = \sigma_0^{a,b} \left[1 - \exp \left(- \frac{r_{\text{eff}}^2}{4R_0^2(x_{ab})} \right) \right]. \quad (20)$$

Here, the saturation radius is defined as

$$R_0(x_{ab}) = \frac{1}{Q_0} \left(\frac{x_{ab}}{x_0} \right)^{-\lambda/2} \quad (21)$$

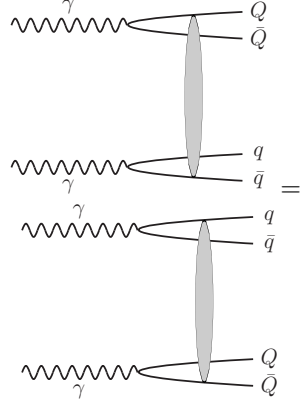


Figure 11. Representative diagrams for $Q\bar{Q}q\bar{q}$ production. The oval in the figure means a complicated interaction which is described here in the saturation model as explained in the main text.

and the parameter x_{ab} which controls the energy dependence was given by

$$x_{ab} = \frac{4m_a^2 + 4m_b^2}{W_{\gamma\gamma}^2}. \quad (22)$$

The effective radius is parametrized as $r_{\text{eff}}^2 = (\rho_1 \rho_2)^2 / (\rho_1 + \rho_2)$ [21]. Some other parametrizations of the dipole–dipole cross section were discussed in the literature. The cross section for the $\gamma\gamma \rightarrow Q\bar{Q}q\bar{q}$ process here is much bigger than the one corresponding to the tree-level Feynman diagram as it effectively resums higher-order QCD contributions.

As discussed in Ref. [22] the $Q\bar{Q}q\bar{q}$ component have very small overlap with the single-resolved component because of quite different final state, so adding them together does not lead to double counting. The cross section for the single-resolved contribution can be written as:

$$\sigma_{1-res}(s) = \int dx_1 [g_1(x_1, \mu^2) \hat{\sigma}_{g\gamma}(\hat{s} = x_1 s)] + \int dx_2 [g_2(x_2, \mu^2) \hat{\sigma}_{\gamma g}(\hat{s} = x_2 s)], \quad (23)$$

where g_1 and g_2 are gluon distributions in photon 1 or photon 2 and $\hat{\sigma}_{g\gamma}$ and $\hat{\sigma}_{\gamma g}$ are elementary cross sections. In our evaluation we take the gluon distribution from Ref. [23].

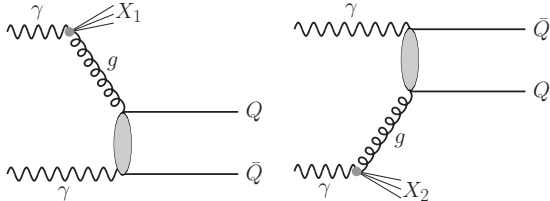


Figure 12. Representative diagrams for the single-resolved mechanism. The shaded oval means either t- or u- diagrams shown in Fig. 9.

Elementary cross sections have been presented and discussed in Ref.[4]. Here we show only nuclear cross sections. In Fig. 13 we compare the contributions of the different mechanisms as a function of the photon-photon subsystem energy. For the Born case it is identical as a distribution in quark-antiquark invariant mass. In the other cases the photon-photon subsystem energy is clearly different than the $Q\bar{Q}$ invariant mass. These distributions reflect the energy dependence of the elementary cross sections. Please note a sizable contribution of the leading-order corrections close to the threshold and at large energies for the $c\bar{c}$ case. Since in this case $W_{\gamma\gamma} > M_{Q\bar{Q}}$, it becomes clear that the $Q\bar{Q}q\bar{q}$ contributions must have much steeper dependence on the $Q\bar{Q}$ invariant mass than the direct one which means that large $Q\bar{Q}$ invariant masses are produced mostly in the direct process. In contrast, small invariant masses (close to the threshold) are populated dominantly by the four-quark contribution. Therefore, measuring the invariant mass distribution one can disentangle some of the different mechanisms. As far as this is clear for the $c\bar{c}$ it is less transparent and more complicated for the $b\bar{b}$ production. In the last case the experimental decomposition may be in practice not possible.

Finally in Table 1 we show partial contribution of different subprocesses discussed above.

3.5. Final comment

We have presented four examples of processes that could be studied at RHIC or LHC. In all cases sizeable cross sections have been obtained. Corresponding measurements are not easy as one has to assure exclusivity of the process, i.e., it must be checked that there are no other particles than that measured in central detectors. In all cases fissibility studies, in-

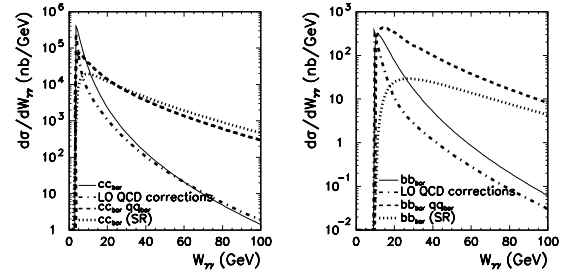


Figure 13. The nuclear cross section as a function of photon-photon subsystem energy $W_{\gamma\gamma}$ in EPA. The solid line denotes the results corresponding to the Born amplitude ($c\bar{c}$ -left panel and $b\bar{b}$ -right panel). The leading-order QCD corrections are shown by the dash-dotted line. For comparison we show the differential distributions in the case when an additional pair of light quarks is produced in the final state (dashed lines) and for the single-resolved components (dotted line).

Table 1

Partial contributions of different mechanisms at $\sqrt{s_{NN}} = 5.5$ TeV.

	σ_{tot}	Born	QCD-corr.	4-q	Sin.-res.
$c\bar{c}$	2.47 mb	42.5 %	14.6 %	27.1 %	15.8 %
$b\bar{b}$	10.83 μ b	18.9 %	7.7 %	64.5 %	8.9 %

cluding Monte Carlo simulations, are required.

Acknowledgments The results presented here were obtained in collaboration with Mariola Klusek, Wolfgang Schäfer, Valerij Serbo and Magno Machado.

REFERENCES

1. G. Baur, K. Hencken, D. Trautmann, S. Sadovskiy and Y. Kharlov, Phys. Rep. **364** (2002) 259; A. Baltz et al., Phys. Rep. **458** (2008) 1.
2. M. Klusek, W. Schäfer and A. Szczurek, Phys. Lett. **B674** (2009) 92.
3. M. Klusek-Gawenda and A. Szczurek, Phys. Rev. **C82** (2010) 014904.
4. M. Klusek-Gawenda, A. Szczurek, M. Machado and V. Serbo, Phys. Rev. **C83** (2011) 024903.
5. M. Luszczak and A. Szczurek, arXiv:1103.4268,

- Phys. Lett. **B700** 116.
6. M. Khusek-Gawenda and A. Szczurek, arXiv:1104.0571. Phys. Lett. **B700** (2011) 322.
 7. R.C. Barrett and D.F. Jackson, "Nuclear Sizes and Structure", Clarendon Press, Oxford 1977.
 8. H. de Vries, C.W. de Jager and C. de Vries, Atomic Data and Nuclear Data Tables, **36** (1987) 495.
 9. J.D. Jackson, Classical Electrodynamics, 2nd ed. (Wiley, New York, 1975), p. 722.
 10. R.N. Cahn and J.D. Jackson, Phys. Rev. **D42** (1990) 3690.
 11. K. Hencken, D. Trautmann and G. Baur, Phys. Rev. **A49** (1994) 1584.
 12. S. J. Brodsky and G. P. Lepage, Phys. Rev. **D24** (1981) 1808.
 13. C. R. Ji and F. Amiri, Phys. Rev. **D42** (1990) 3764.
 14. A. Szczurek and J. Speth, Eur. Phys. J. **A18** (2003) 445.
 15. S. J. Brodsky and G. P. Lepage, Phys. Lett. **B87** (1979) 359.
 16. A.V. Efremov and A. V. Radyushkin, Phys. Lett. **B94** (1980) 245.
 17. V. L. Chernyak and A. R. Zhitnitsky, Nucl. Phys. **B201** (1982) 492.
 18. X. G. Wu and T. Huang, Phys. Rev. **D82** (2010) 034024.
 19. M. Diehl, P. Kroll and C. Vogt, Phys. Lett. **B532** (2002) 99; M. Diehl and P. Kroll, Phys. Lett. **B683** (2010) 165.
 20. B.A. Kniehl, A.V. Kotikov, Z.V. Merebashvili and O.L. Veretin, Phys. Rev. **D79** (2009) 114032.
 21. N. Timneanu, J. Kwiecinski and L. Motyka, Eur. Phys. J. **C23** (2002) 513-526.
 22. A. Szczurek, Eur. Phys. J. **C26** (2002) 183-194.
 23. M. Gluck, E. Reya and A. Vogt, Phys. Rev. **D46** (1992) 1973.